SOILS AND FOUNDATIONS Vol. 45, No. 4, 133-147, Aug. 2005
Japanese Geotechnical Society

SEISMIC EFFECTIVE-STRESS ANALYSIS OF CAISSON QUAY WALLS: APPLICATION TO KOBE

P. DAKOULAS[i] and G. GAZETAS[ii]

ABSTRACT

Deformation-based seismic design of gravity quay-walls requires realistic computation of residual deformations. This article presents an effective-stress analysis method, which is based on an elasto-plastic constitutive model formulated into a finite-difference algorithm. The model is applicable to cohesionless soils, for a wide range of relative densities and confining pressures. The formulation is applied first to re-analyze one of the failed caisson-type quay-walls of Rokko Island during the 1995 Kobe (Hyogoken-nambu) earthquake (Case 1). Subsequently, it is applied to analyse three closely related case studies of quay-walls, subjected to the same earthquake excitation, to demonstrate the effects of ground improvement on the wall performance. Case 2 considers a quay-wall in which both the foundation and backfill consist of improved, non-liquefiable soils. Case 3 considers a quay-wall in which the backfill soil remains liquefiable, whereas the foundation soil has been improved. Finally, in Case 4 the foundation soil is liquefiable, and the backfill soil improved. The results are consistent with both field observations and earlier independent computer simulations by Iai et al. 1998 which were based on the finite-element method and a different constitutive model.

Key words: caisson wall, case history, constitutive model, earthquake, effective stress, harbor, Kobe, liquefaction, pore pressures, quay-wall (**IGC**: E8/E13)

INTRODUCTION

The failures of caisson quay-walls in 1995 Kobe (Hyogoken-nambu) earthquake provided the motivation for substantial progress in the development of deformation-based design methods for waterfront structures. Significant theoretical and experimental research work has been published on the subject (Inagaki et al., 1996; Ishihara et al., 1996; Ishihara, 1997; Kamon et al., 1996; Towhata et al., 1996; Iai 1998; Iai et al., 1998; Dickenson et al., 1998; Ghalandazadeh et al., 1998; Sekiguchi et al., 1999; Sawada and Kondoh, 1999; Tazoh and Gazetas, 1996). Advanced constitutive models and large deformation effective-stress numerical procedures have been developed and used extensively in analysis of recorded case histories and in comprehensive parametric studies. The results of these research efforts were generally in good agreement with existing field observations. Some of these findings have been coded in the PIANC (2001) manual.

To enhance the reliability of such numerical simulations, extend their applicability to a wide range of soil cyclic behavior, develop a deeper understanding into the mechanics of the problem, and draw conclusions of practical significance, additional research is needed focusing on improving the effective stress methods and on analyzing case histories of both good and bad performance. To help in meeting these objectives, this paper introduces a new method for large-deformation analysis of gravity caisson-type quay-walls retaining or founded on liquefiable or non-liquefiable soils.

The research is based on an elasto-plastic constitutive model that can simulate the monotonic and cyclic behavior of a cohesionless soil in a wide range of relative densities and confining pressures. The constitutive model has been incorporated into the finite-difference code FLAC (Itasca, 2000), and verified through comparisons with existing laboratory testing data and analysis of case histories. The numerical formulation is then used in parametric investigations of various caisson quay-wall systems. The objective of this study is to evaluate the effect of key parameters on the size of residual deformations of gravity quay-walls, and thereby to develop rational improvement measures (e.g., by modification of the geometry and the foundation and backfill soil properties). This article focuses on the analysis of a typical Rokko Island caisson quay-wall failure during the 1995 Kobe earthquake, and on three case studies involving improved ground. The results are compared with field observations and the results of Iai et al. (1998), who used a different soil constitutive model and a different numerical formulation.

[i] Department of Civil Engineering, University of Thessaly, Volos, Greece.
[ii] School of Civil Engineering, National Technical University of Athens, Greece (gazetas@ath.forthnet.gr).
The manuscript for this paper was received for review on March 17, 2004; approved on May 30, 2005.
Written discussions on this paper should be submitted before March 1, 2006 to the Japanese Geotechnical Society, 4-38-2, Sengoku, Bunkyo-ku, Tokyo 112-0011, Japan. Upon request the closing date may be extended one month.

METHOD OF ANALYSIS AND CONSTITUTIVE MODEL

The constitutive model for cohesionless soils adopted in the present study is the one developed by Pastor et al. (1990), after some minor modifications explained below. The model has been developed in the framework of generalized plasticity, and avoids some complexities associated with classical plasticity. It is based on critical-state theory, which postulates that all residual states lie on an unique line on the $p'-q-e$ space, regardless of the followed stress path. Consistently with experimental evidence for cohesionless soils, the model uses a non-associative flow rule for the unstable behavior within the hardening region. An advantage of the model is that it does not require the explicit definition of the yield and potential functions, but only of the direction vectors normal to each surface. Also, it does not require the application of the so-called *"consistency" condition* to define the hardening modulus.

The stress-strain relationship is given by;

$$d\sigma' = D^{ep}_{L/U}\, d\varepsilon = \left(D^e - \frac{D^e n_{gL/U}\, n D^e}{H_{L/U} + n^T D^e n_{gL/U}} \right) d\varepsilon \tag{1}$$

where $d\sigma'$ = the stress increment; $d\varepsilon$ = the strain increment; $D^{ep}_{L/U}$ = the elastoplastic stiffness matrix for loading/unloading; D^e = the elastic stiffness matrix; $H_{L/U}$ = the plastic modulus for loading/unloading; n = the loading direction; $n_{gL/U}$ = the direction of the plastic strain increment. The vector $n_{gL/U}$ is given *for loading* by;

$$n^T_{gL} = \frac{(d_g, 1, -0.5\, M_g q \cos 3\theta)}{\sqrt{d_g^2 + 1 + (0.5\, M_g q \cos 3\theta)^2}} \tag{2}$$

and *for unloading* by;

$$n^T_{gU} = \frac{(-|d_g|, 1, -0.5\, M_g q \cos 3\theta)}{\sqrt{d_g^2 + 1 + (0.5\, M_g q \cos 3\theta)^2}} \tag{3}$$

where d_g is the soil dilatancy expressed as;

$$d_g = \frac{d\varepsilon^p_v}{d\varepsilon^p_s} = (1+\alpha)(M_g - \eta) \tag{4}$$

and

$$\eta = \frac{q}{p'} \tag{5}$$

$$p' = (\sigma'_{11}\sigma'_{22} + \sigma'_{33})/3 \tag{6}$$

$$q = \sqrt{3J_2} \tag{7}$$

$$M_g = \frac{6\, M_{gc}}{6 + M_{gc}(1 - \sin 3\theta)} \tag{8}$$

$$\theta = \frac{1}{3} \sin^{-1}\left(\frac{3\sqrt{3}J_3}{2J_2^{3/2}} \right) \text{ (Lode angle)} \tag{9}$$

J_2, J_3 = the second and third deviatoric stress invariants, respectively.

M_{gc}, α = model parameters.

The normal to the yield surface vector n is given by;

$$n^T = \frac{(d_f, 1, -0.5\, M_f q \cos 3\theta)}{\sqrt{d_f^2 + 1 + (0.5\, M_f q \cos 3\theta)^2}} \tag{10}$$

where

$$d_f = (1+\alpha)(M_f - \eta) \tag{11}$$

$$M_f = \frac{6M_{fc}}{6 + M_{fc}(1 - \sin 3\theta)} \tag{12}$$

and M_{fc} is a model parameter.

The plastic modulus for loading is given by;

$$H_L = H_0 p' H_f (H_v + H_s) H_{DM} \tag{13}$$

where

$$H_f = \left(1 - \frac{\eta}{\eta_f}\right)^4 \tag{14}$$

$$H_v = \left(1 - \frac{\eta}{M_g}\right) \tag{15}$$

$$H_s = \beta_0 \beta_1 e^{-\beta_0 \zeta} \tag{16}$$

$$H_{DM} = \left(\frac{\eta_{max}}{\eta}\right)^{\gamma} \tag{17}$$

$$\eta_f = \left(1 + \frac{1}{\alpha}\right) M_f \tag{18}$$

ζ = accumulated plastic deviatoric strain, and H_0, β_0, β_1 and γ = model parameters.

The plastic modulus for unloading H_U has been modified from the original form (Pastor et al., 1990) in order to incorporate the stress dependency, and is expressed as;

$$H^*_U = \begin{cases} H^*_{uo} p' \left(\dfrac{M_g}{\eta_u}\right)^{\gamma_u}, & \text{if } \left|\dfrac{M_g}{\eta_u}\right| > 1 \\ H^*_{uo} p', & \text{if } \left|\dfrac{M_g}{\eta_u}\right| \le 1 \end{cases} \tag{19}$$

where H^*_{uo}, γ_u are model parameters and η_u is the stress ratio from which unloading takes place.

Finally, the expressions for the stress dependency of the elastic bulk and shear moduli (K and G) have been modified from the original expressions by Pastor et al. (1990) to the form:

$$K = K_0 \left(\frac{p'}{p_o}\right)^m \tag{20}$$

$$G = G_0 \left(\frac{p'}{p_o}\right)^m \tag{21}$$

where K_0, G_0 are material parameters, p_0 is a reference confining pressure, p' is the mean effective stress and m is typically 0.5, but may vary from 0.3 to 1 (in the original model $m=1$). Moreover, it is interesting to note that similar (but not identical) modifications about the stress dependency of the elastic and plastic moduli have been presented independently by Ling et al. (2003), about the same time with this work (Dakoulas, 2003a, b). Detailed descriptions of the basic model are given by Pastor et al. (1990, 1986, 1985) and Zienkiewicz et al. (1999, 1991, 1985).

For loose *contractive* sand, the model predicts the densification and strain hardening undergoing drained shearing, and the development of excess pore pressure and liquefaction undergoing undrained shearing. For

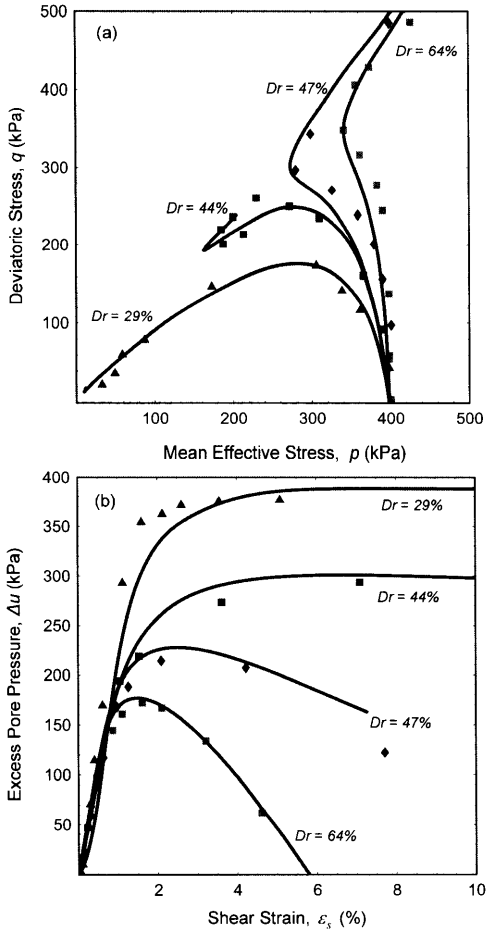

Fig. 1. Comparison of experimental data from Castro (1969) with the numerically computed curves with the extended *Pastor* model: (a) effective stress paths and (b) excess porewater pressures

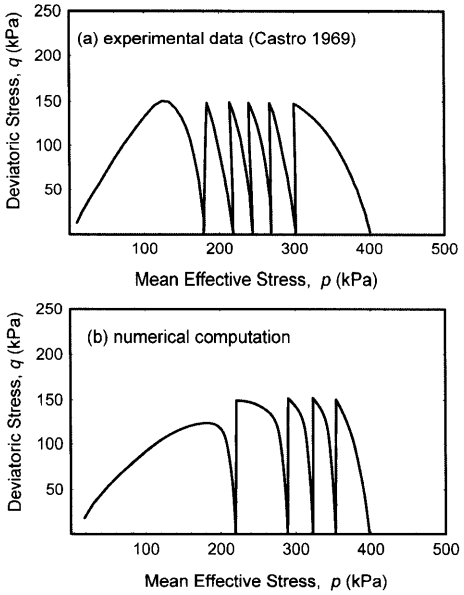

Fig. 2. Effective stress paths in cyclic triaxial testing for a sand with $D_r = 29\%$: (a) experimental data (Castro, 1969) and (b) numerically computed path

very dense *dilative* sands in drained shear, the model accounts for strain softening and residual conditions at the critical state. Comparisons between predictions of the original model and experimental data on undrained monotonic loading of contractive and dilative sands, on cyclic loading leading to liquefaction of very loose sands, and on cyclic mobility of dense sands, showed very good agreement (Pastor et al., 1990). Similarly, verification studies on drained and undrained, monotonic and cyclic, tests on various sands utilising the modified version by Ling et al. (2003) has shown very good agreement with the experimental data.

A systematic series of comparisons between predictions of the modified model presented above and experimental data of different sands from monotonic and cyclic tests in compression-extension has been conducted as part of this study (Dakoulas, 2003b). Figure 1(a) shows a comparison of the effective stress paths during triaxial undrained compression of Banding sand (Castro, 1969) with relative density $D_r = 29\%$, 44%, 47% and 64% using the model described above, whereas Fig. 1(b) compares the corresponding excess pore water pressure versus shear strain curves. Figure 2 compares stress paths during undrained cyclic triaxial testing of a sample with relative density of $D_r = 30\%$. Finally, Fig. 3 compares the Cyclic Stress Ratio (CSR) for initiation liquefaction (i.e. reaching a state of zero effective stress) in simple shear tests from model predictions and experimental data of Nevada Sand (Arulmoli et al., 1992) and Monterey Sand (DeAlba et al., 1976, as modified by Seed and Harder, 1990) for relative densities of 40% and 60%. Overall, the model seems capable of describing realistically the soil behavior under monotonic and cyclic loading for a wide range of relative densities. It is being used to simulate approximately the soil response under seismic conditions. To this end, the model is attached into the well-established finite-difference code, FLAC (Itasca, 2000).

RELATIVE DENSITY FROM FIELD DATA

As a direct evaluation of D_r from undisturbed samples through ground freezing is too costly, a correlation based on field measurements would be a more practical approach in most cases. Experimental evidence shows that the Standard Penetration Test (SPT) resistance of cohesionless soils depends on the grain size and the fines content. Cubrinovski and Ishihara (1999, 2000, 2001) used high-quality undisturbed ground frozen samples and measured SPT resistance of natural soil deposits and developed the following empirical correlation between SPT, N value and relative density, D_r, for a wide range of cohesionless soils:

$$D_r = \{N_1(e_{max} - e_{min})^{1.7}\}^{1/2}/3 \quad (22)$$

where $N_1 = (98/\sigma'_v)^{1/2} N$, σ'_v = the effective vertical stress (kPa), and e_{max}, e_{min} = the limiting values of void ratio. Although the void ratio range is only an indirect measure of gradation, it was found to be a very good indicator of the overall grain-size characteristics of sandy soils. An

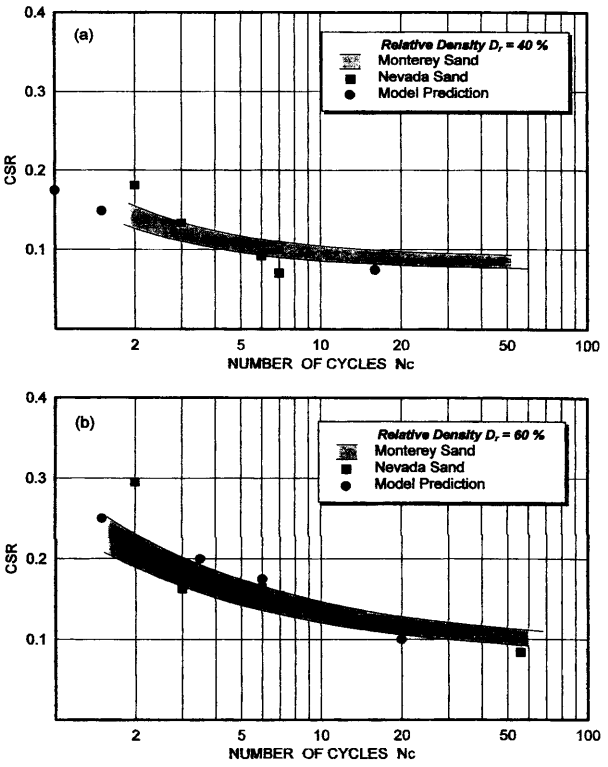

Fig. 3. Cyclic Stress Ratio for initial liquefaction in simple shear tests from model predictions and experimental data for Nevada Sand (Arulmoli et al., 1992) and Monterey Sand (DeAlba et al., 1976, as modified by Seed and Harder, 1990)

approximate relationship between $e_{max} - e_{min}$ and D_{50}, applicable to gravelly sands, clean sands, and sands with fines, may be expressed as (Cubrinovski and Ishihara, 2001):

$$e_{max} - e_{min} = 0.23 + 0.06/D_{50} \quad (23)$$

The relative density, D_r, required by our constitutive model is estimated from Eq. (1) and subsequently corrected through laboratory cyclic strength data, when of course such data are available for the given site.

CASE HISTORIES AND CASE STUDIES

During the strong shaking of the 1995 Kobe (Hyogoken-nambu) earthquake the caisson type waterfront structures at the port of Kobe suffered substantial damage in the form of large seaward displacement and rotation (Inagaki et al., 1996). However no overturning failures occurred. These caisson walls had been designed pseudo-statically with seismic coefficients ranging from 0.10 to 0.25, depending on site conditions, year of construction, and importance of the facility. They had been placed on top of gravelly fill consisting of decomposed granite (called locally "Masado"), which had completely replaced the soft clay layer beneath the caisson for improving the bearing capacity and reducing settlements. The most severe damage occurred in those caisson walls of Port and Rokko Islands were nearly parallel to the coast-line (and thus to the causative fault) and those which had been designed with small seismic coefficients, of 0.10 to 0.15 only.

By contrast, the caisson wall of the main wharf at Maya Futo, designed conservatively with a seismic coefficient equal to 0.25 and running almost perpendicular to the fault, did not experience any visible damage or deformation, remaining operational after the earthquake. It is worth mentioning here that despite the large deformations, the caisson walls did not overturn. Their overall performance can be judged as better than that of the alternative quay-wall system, the anchored sheet-pile wall, which in earlier but much less devastating earthquakes than Kobe, were frequently experiencing collapsing failures (e.g., Kitajima and Uwabe, 1977; Gazetas and Dakoulas, 1990).

The effective-stress method is applied here to analyze one case history and three closely related case studies of quay-walls, subjected to the actual horizontal and vertical accelerations recorded in the renown seismic array at Port Island. Our objectives are: (a) to evaluate the performance of the method, (b) to develop a deeper understanding on the mechanics of caisson displacements, and (c) to investigate the effects of ground improvement strategies on quay-wall response. The case history (Case 1) corresponds to the typical quay-wall section of Rokko Island, in which both the foundation and backfill soils are liquefiable. Case 2 considers a quay-wall section in which both the foundation and backfill consist of ideally improved, non-liquefiable soils. Next, Case 3 considers a section in which the backfill soil is liquefiable, whereas the foundation soil has been improved. (This case represents, even if crudely, the conditions at quay-wall sections PC-14 and 15 of Port Island according to Iai et al., 1998.) Finally, Case 4 considers a section in which the foundation soil is liquefiable, but the backfill soil has been improved.

Case History 1: Rokko Island Quay-Wall Displacement

A cross-section of the quay-wall RC-5 with its deformation recorded after the earthquake is reproduced in Fig. 4(a), from Iai et al. (1998). The finite-difference discretization and the material zones used in our analyses are shown in Fig. 4(b). During the earthquake, the wall top displaced approximately 4 m seaward (but more than 5 m in some locations). It settled about 1 to 2 m and tilted about 4 degrees outward. Despite these significant movements, the site investigation showed no collapse of the wall along its entire length. Also, no evidence was observed of liquefaction either within the zone extending about 30 m behind the wall or near the toe of the wall in the sea, but such evidence was produced farther away in the free field (Towhata et al., 1996; Iai et al., 1998; Inagaki et al., 1996). Investigation by divers cited by Inagaki et al. (1996) revealed substantial heaving of the foundation rubble at a distance 2 to 5 meters in front of the toe of the caisson—indicative of "*squeezing out*" of the soil underneath the edge (toe) of the tilting caisson.

Detailed information about SPT-N values at various depths, grain-size distribution, S-wave velocities, and

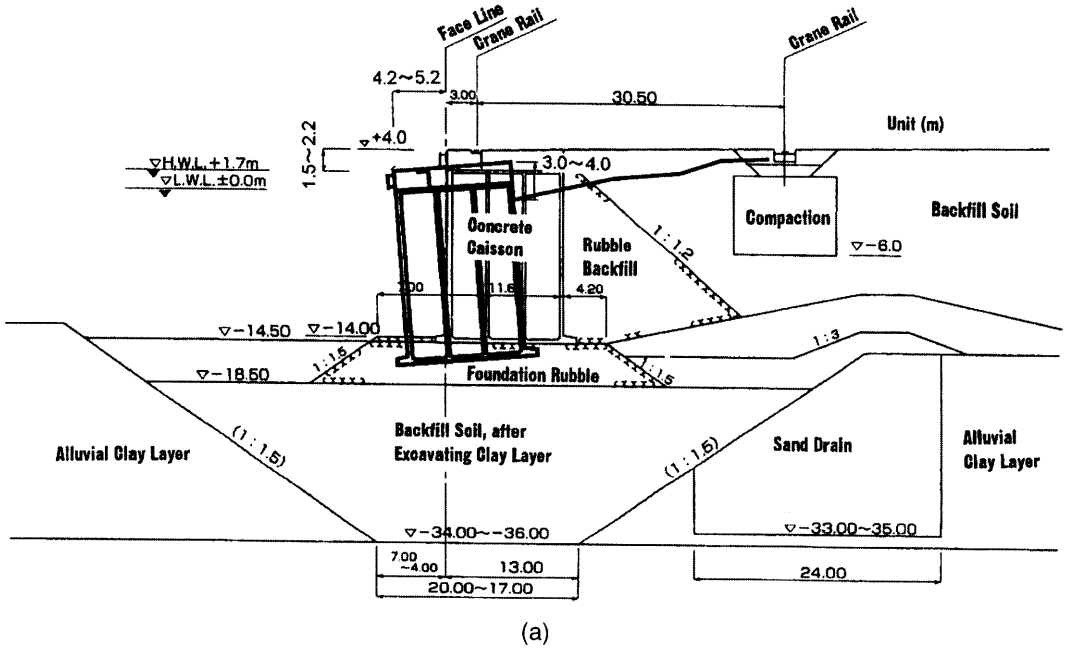

Fig. 4(a). Cross section of the caisson quaywall RC-5 in Rokko Island and its residual deformation observed after the Kobe 1995 Earthquake (from Iai et al., 1996)

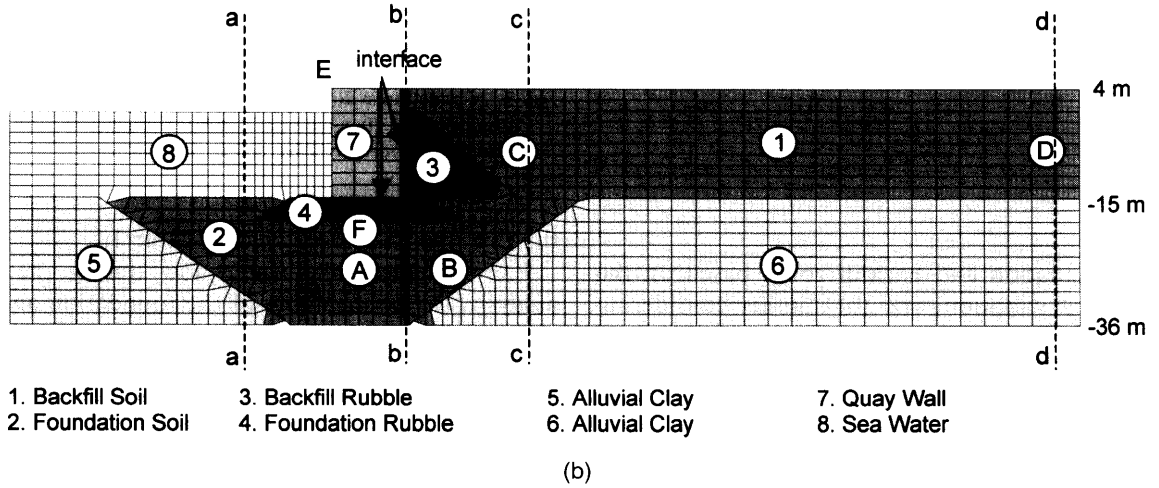

Fig. 4(b). Case 1: Geometry (in natural scale), finite-difference discretization, and material zones of the Rokko Island quay-wall system: Points A, B, C and D and lines aa, bb, cc, and dd, are for showing details of porewater pressures and displacements

cyclic triaxial test data have been presented by Inagaki et al. (1996). The density, initial shear modulus, and friction angle in Table 1 were taken from Iai et al. (1998). The materials in the backfill, foundation, backfill rubble, and foundation rubble zones were modeled with the *modified Pastor* model. The relative density of the material is estimated from the SPT blow counts and the material characteristics (Inagaki et al., 1996), including the relatively high contractiveness of the decomposed granite material (Torii and Tatsuoka, 1982). Figure 5 plots the Cyclic Stress Ratio,

$$\mathrm{CSR} = (\sigma_1 - \sigma_3)/2\sigma_c' \tag{24}$$

where σ_c' is the confining effective stress, obtained from triaxial tests. The tests were performed on soil samples obtained by freezing from (a) backfill soil and (b) replaced sand in Rokko Island, and then consolidated to confining pressures equal to the *in-situ* vertical effective stresses (Inagaki et al., 1996). The results are plotted against the number of cycles, N_c, required to cause 2%, 5% and 10%, double amplitude axial strain. Also shown in this figure are the model predictions of the CSR versus number of cycles required to cause 10% axial strain, for $D_r = 35\%$. Note that for $N_c < 7$ cycles the real soil is more contractive than the model, whereas for $N_c > 7$ the real soil is less contractive.

Two types of analyses were performed during this investigation: (a) one considering a variable relative density

Table 1. Material properties for Case 1 (After Iai et al., 1998)

Material	Density Mg/m^3	G_{max} MPa	σ'_0 kPa	φ degrees
Foundation, Zone 2	1.8	58	106	37
Backfill, Zone 1	1.8	79	63	37
Alluvial clay, Zones 5, 6	1.7	75	143	30
Rubble, Zones 3, 4	2	80	98	40
Caisson wall	2.1			

Friction angle at caisson bottom = 30°, Friction angle at caisson back = 15°

Table 2. Model parameters for relative densities $D_r = 35\%$ and 75%

Material parameter	$D_r = 35\%$	$D_r = 75\%$
K_0	34000	45000
G_0	17500	23200
M_{gc}	1.42	1.08
M_{fc}	0.34	0.74
α	0.45	0.50
H_0	350	800
β_0	6	6
β_1	0.76	0.6
γ	4	4
H_{u0}	2000	2000
γ_u	2	2

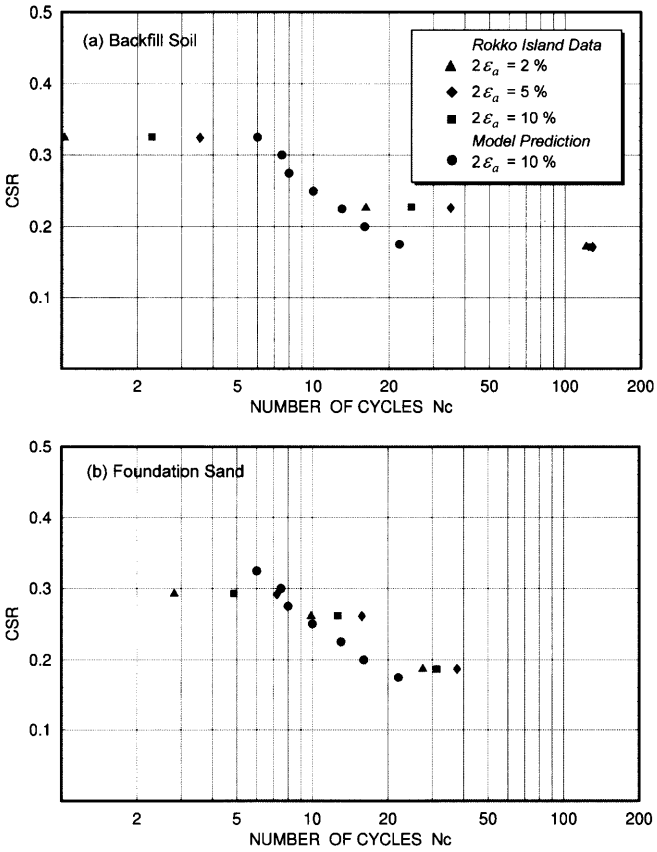

Fig. 5. Cyclic Stress Ratio (CSR) from triaxial tests on samples from Rokko Island (Inagaki et al., 1996): Comparison with predictions using our model, Relative density $D_r = 35\%$

within the foundation and backfill zones based on the SPT blow count variation, and (b) another considering an uniform distribution of an equivalent relative density of 35%. No significant differences were noted in the results. Thus, only those from the uniform distribution are presented here. Although the value of $D_r = 35\%$ is admittedly an approximation, given the variability in density of the decomposed granite soil, it is adopted here in order to simplify the interpretation, and thereby allow an easier comparison between the response of natural and improved soil. In fact, comparisons between the computed and actual response discussed below, indicate that in a significant part of the quay-wall in Rokko Island, the equivalent relative density of the foundation or backfill soil might have been even lower than 35%.

The clay zones are modeled approximately using the Mohr-Coulomb model with properly adjusted material parameters based on independent equivalent linear analysis. The sea water mass is modeled as a saturated, elastic sponge, having the density and the bulk modulus of the water, and an artificial, very small value of the shear modulus that is necessary to avoid numerical problems.

Finally, the wall is modeled as an elastic body, having an interface that allows slippage and separation at the base and the back of the caisson. The friction angles at the two interfaces are given in Table 1.

For simulating the water flow during the dynamic analysis, the permeability of the foundation and backfill soil is taken equal to $k = 4 \times 10^{-5}$ m/s, for the rubble material $k = 4 \times 10^{-4}$ m/s and for the clay $k = 10^{-8}$ m/s. Drainage is allowed at the base of the sea in front of the wall and at the water table level at the backfill soils. A static consolidation analysis is conducted to establish the initial static stresses before the earthquake loading.

For the seismic excitation of our model we also adopted the (logical) choice of many researchers, including Iai et al. (1998): the horizontal (NS) and vertical components of the accelerogram recorded at a depth of 32 m in the renowned Port Island array (Iwasaki and Tai, 1996), whose peak acceleration values reached 0.54 g and 0.20 g, respectively.

Figures 6(a) and 6(b) plot the accelerogram components whereas Fig. 6(c) plots the corresponding acceleration response spectra. The choice is reasonable in view of the proximity (in relative terms) of the two sites (in Port and Rokko islands) and the similarity in stiffness of the underlying soil where the record is applied. It is noted, however, that due to substantial *forward-rupture directivity* effects in the Kobe earthquake, ground motions normal to the fault were significantly stronger (in long-period components) than fault-parallel motions; hence the orientation of a particular wall is important in choos-

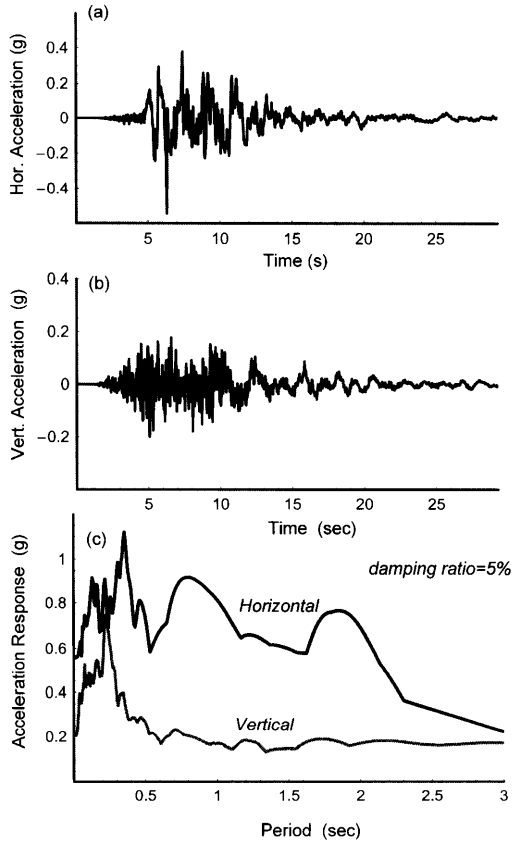

Fig. 6. Input Excitation: the two components of ground motion recorded in the Port Island Seismograph Array at the depth of 32 m, during the 1995 Kobe earthquake: (a) horizontal NS component, (b) vertical component, and (c) the corresponding acceleration response spectra for critical damping ratio equal to 5% (Adapted from Iwasaki and Tai, 1996)

ing the probable excitation. Therefore, the choice of excitation unavoidably introduces some uncertainty in our results.

The horizontal and vertical components of excitation are applied at the depth of -36 m, whereas free-field conditions are applied by the numerical formulation at the left and the right vertical boundaries of the model.

Figure 7 portrays the contours of horizontal displacement (Fig. 7(a)) and excess porewater pressure (Fig. 7(b)) at the end of shaking i.e. at $t = 30$ seconds. (The sea-water mesh has been removed from the plot for clarity.) Figure 7(a) should be studied along with Fig. 8(a), which plots the time history of the horizontal and vertical displacements at the upper left (seaside) corner of the wall, and Fig. 8(b), which shows the distribution of horizontal displacements with depth at four vertical lines (aa, bb, cc, and dd, indicated in Fig. 4(b)).

It is noted that at the end of the earthquake, the seaside corner of the wall is computed to have moved by about 3.7 m horizontally and settled 1.3 m. However, the wall continued to move horizontally even after the first 30 seconds of the shaking, reaching gradually a final value of about 3.95 m. The deformed mesh in Fig. 7(a) shows that the retained soil behind the wall settled significantly (with a maximum settlement about 2.1 m), following the seaward movement of the wall. These displacements are in excellent accord with the field observations.

Moreover, the foundation rubble was substantially deformed at the left side as can be discerned in Fig. 7(a) and in the profile aa in Fig. 8(b). Notice that the deformation of the foundation soil beneath the caisson caused most of the horizontal movement of the wall; no sliding was computed between the caisson base and the foundation rubble. The deformation pattern of the foundation rubble indicates a reduced bearing capacity of the

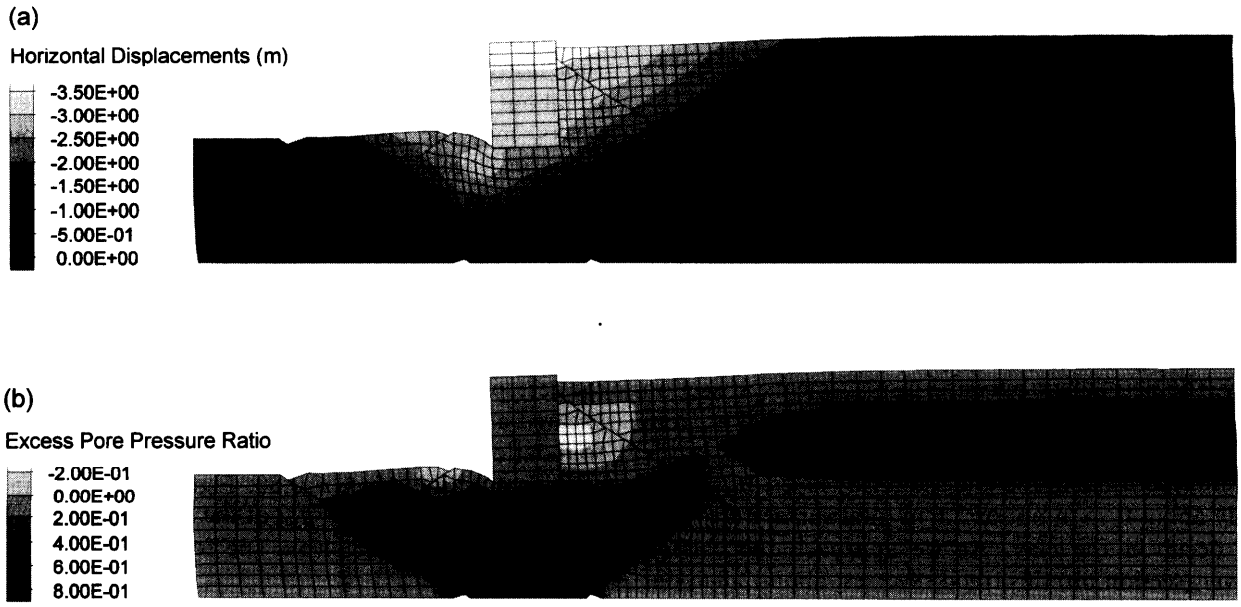

Fig. 7. Case 1: (a) deformed geometry and contours of horizontal displacements of the quay wall at the end of shaking ($t = 30$ sec) and (b) deformed geometry and contours of excess porewater pressure ratio at the end of shaking ($t = 30$ sec)

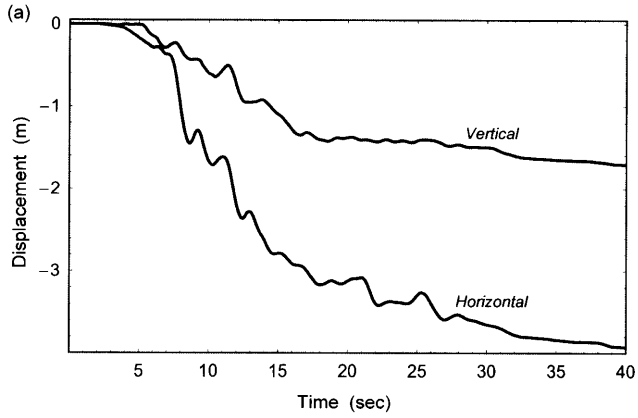

Fig. 8(a). Case 1: Rokko Island quay-wall: Computed horizontal and vertical displacement time histories at the upper seaside corner of the caisson (point E of Fig. 4(b) and (b) Distribution of horizontal displacement along sections aa, bb, cc and dd at the end of shaking ($t = 30$ sec)

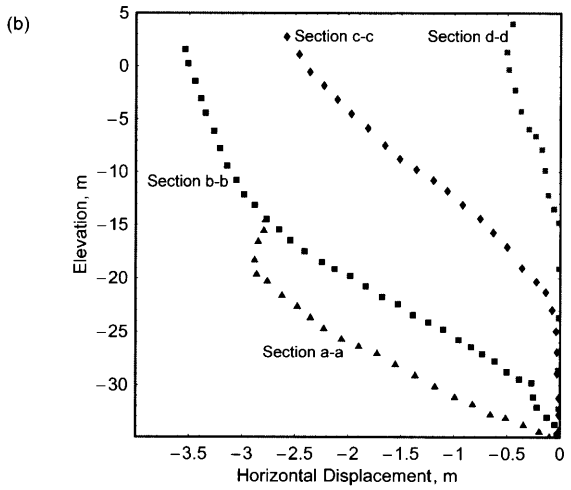

Fig. 8(b). Case 1: Rokko Island quay-wall: Computed horizontal and vertical displacement time histories at the upper seaside corner of the caisson (point E of Fig. 4) and (b) Distribution of horizontal displacement along sections aa, bb, cc and dd at the end of shaking ($t = 30$ sec)

foundation soil under significant moment loading from the heavy and tall wall. Such a reduction in bearing capacity appears to be an important deformational mechanism that contributed significantly to the large rotation of the wall.

Several other observations can be made from Fig. 8(b): Firstly, the permanent outward displacements at section dd (free field) and even at section cc (merely 22 m from the back of the wall) are primarily displacements in the backfill rather than in the underlain clay layer. In section cc only about 0.75 m out of 2.6 m total surface displacement occur in the clay. As we approach the caisson however (section bb) this trend reverses: about 2.8 m out of the 3.6 m total top displacement already take place in the decomposed granite fill beneath the caisson wall.

Secondly, we notice in Fig. 7(a) that the computed

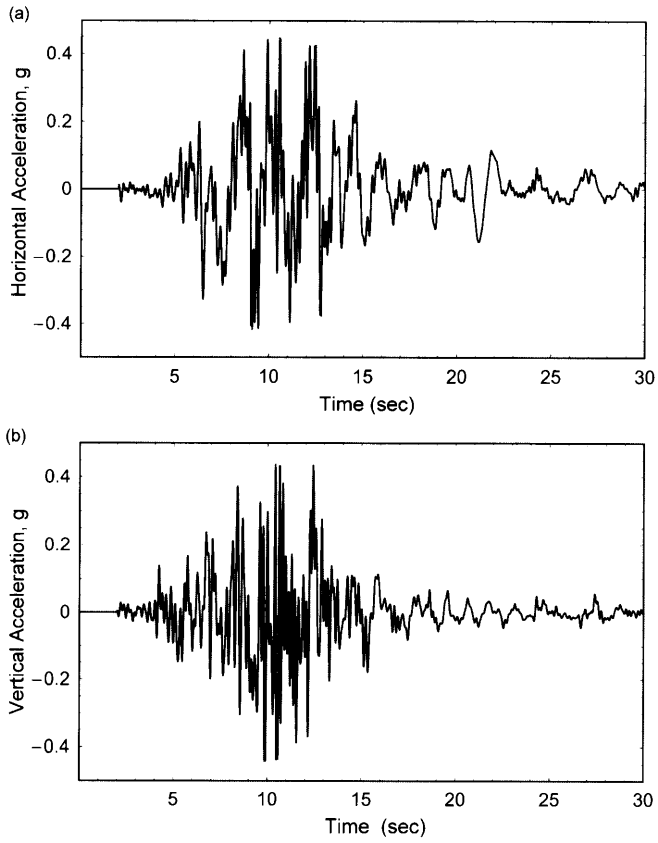

Fig. 9. (a) Case 1: Rokko Island quay-wall: Computed (a) horizontal and (b) vertical acceleration time histories at the upper seaside corner of the caisson (point E of Fig. 4(b))

permanent outward displacement at the backfill surface extends all the way to the end of our model, at about 100 m from the wall (displacement ≈ 0.40 m). This is consistent with the observation of the extent of lateral spreading over distances of 100 m–200 meters from the quay-walls (Ishihara, 1997).

Figure 9 plots the horizontal and vertical acceleration time histories at point E (Fig. 4(b)), with both peak values of about 0.44 g. Note, however, that the acceleration peaks may be affected by high-frequency spurious numerical peaks that would overestimate the maximum acceleration response.

Figure 7(b) plots the contours of excess porewater pressure ratio, $\Delta u/\sigma'_{0m}$, where Δu = the excess porewater pressure and σ'_{0m} = the initial mean effective stress. The results show that high porewater pressure ratios develop both in the free field *and* beneath the caisson. Moreover, the left part of the foundation soil is compressed and sheared as the left side of the wall settles deeper into the foundation soil, where the excess pore water pressure ratios reach the value of 0.80. Figure 10 plots the time histories of the ratio $\Delta u/\sigma'_{0m}$ at the four points, A, B, C, and D, shown in Fig. 4(b). The following observations are noteworthy:

- The highest excess porewater pressure ratio, of about 0.90, develops in the free field point D. Notice the relatively slow rate of pressure accumulation.

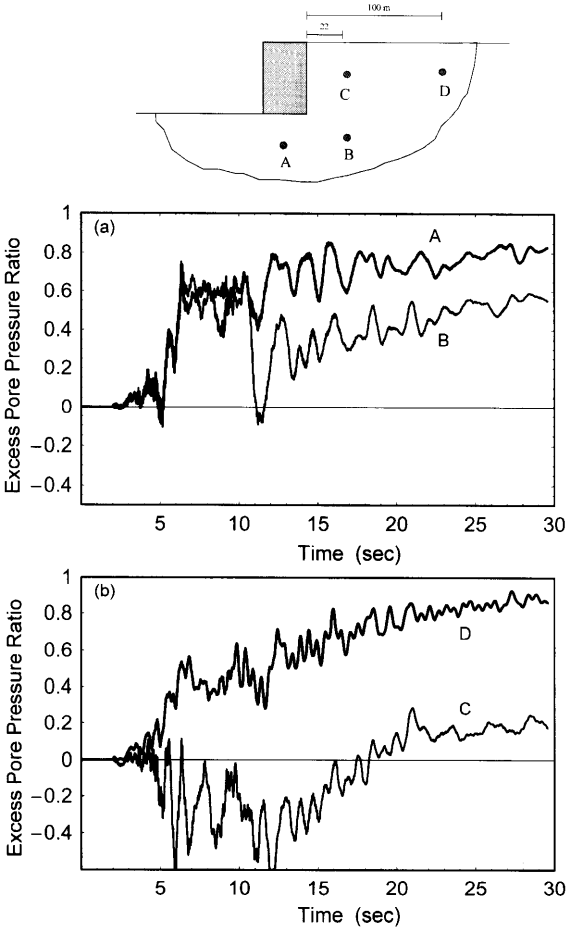

Fig. 10. Case 1: Computed time histories of excess porewater pressure ratio, $\Delta u/\sigma'_{0m}$, at points A, B, C, and D

- By contrast, in the backfill point C, located at the same depth as D but only 22 m from the back of the wall, the excess pore pressure ratio attains large negative values (≈ -0.60) with strongly oscillatory behavior during the period of the strong shaking; at $t \approx 14$ sec it starts increasing, and gradually accumulates to a level of about $+0.20$. This behavior is due to the stress relaxation that develops in this region as the wall moves outward (seaward) and the associated dilative response of the soil arising from both the confining stress reduction and shearing. Notice that the big negative increments in porewater pressure occur at about 6 and 12 seconds, when the long-duration acceleration pulses in the excitation (Fig. 6) cause the outward wall movement.
- Point B exhibits a porewater pressure response of intermediate nature, between the responses of C and D. From 6 to 10 sec $\Delta u/\sigma'_{vm}$ reaches a plateau of about 0.60. (*see* explanation below). At time $t \approx 11$ sec, when there is a significant increase in the rate of seaward movement of the wall, a significant temporary reduction takes place, after which the ratio gradually approaches the residual value of 0.60.
- Point A, located on the caisson centerline at about 12 m underneath its base, develops a $\Delta u/\sigma'_{vm}$ ratio of about 0.60 very quickly after $t \approx 5.0$ sec (compared with the slower build-up in the free-field point D). This is believed to be the result of the sustained large inertia force apparently experienced by the wall and the backfill due to the arrival of the first long-duration acceleration pulses of the excitation at $t \approx 5.0$–6.0 seconds. Eventually the ratio slowly approaches again to the value of 0.80.

The overall response is consistent with the observed

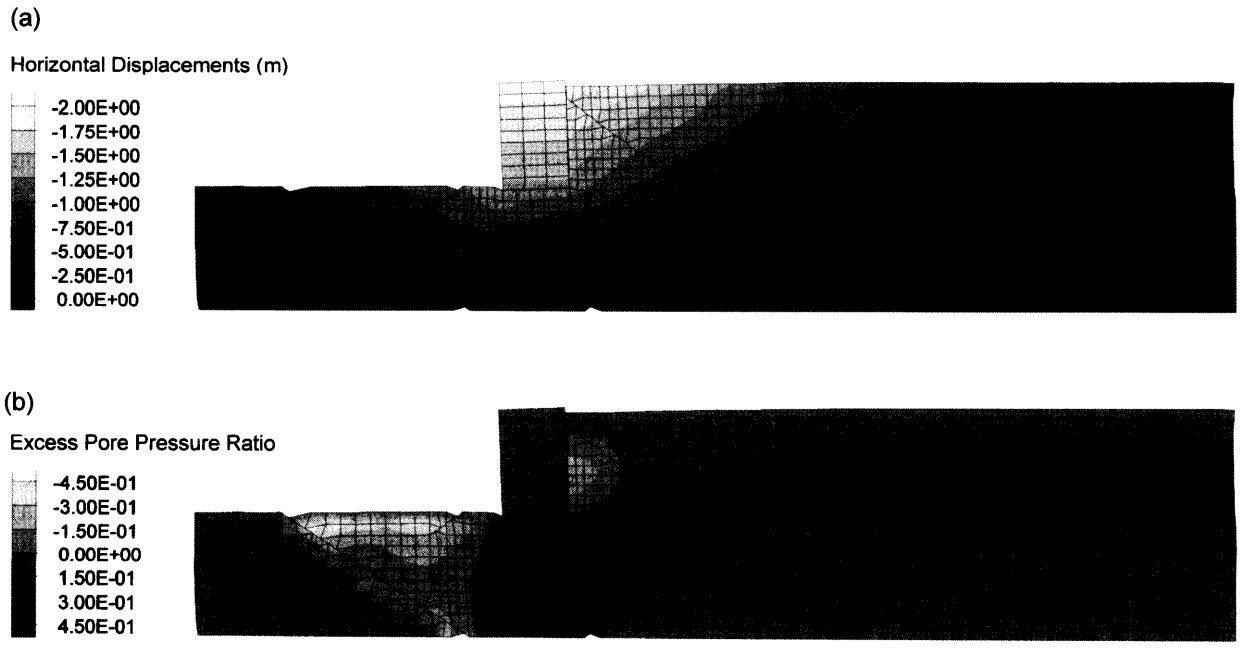

Fig. 11. Case 2: Densified soil of the backfill ($D_r = 75\%$) and the foundation ($D_r = 75\%$): (a) Deformed geometry and contours of horizontal displacements of the quay-wall at the end of shaking ($t = 30$ sec) and (b) Deformed geometry and contours of excess porewater pressure ratio at the end of shaking ($t = 30$ sec)

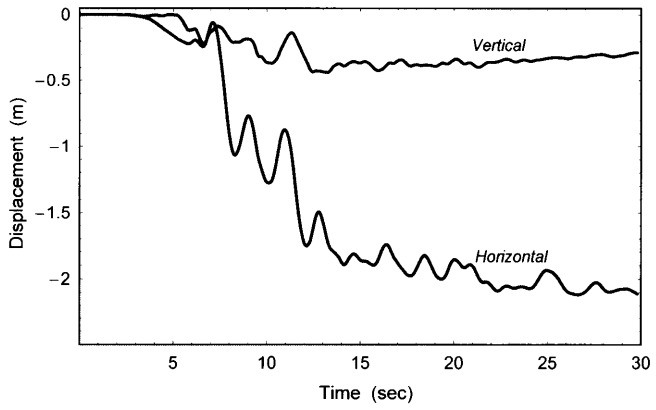

Fig. 12. Case 2: Densified soil of the backfill ($D_r = 75\%$) and the foundation ($D_r = 75\%$): Computed horizontal and vertical displacement time histories at the upper seaside corner of the wall

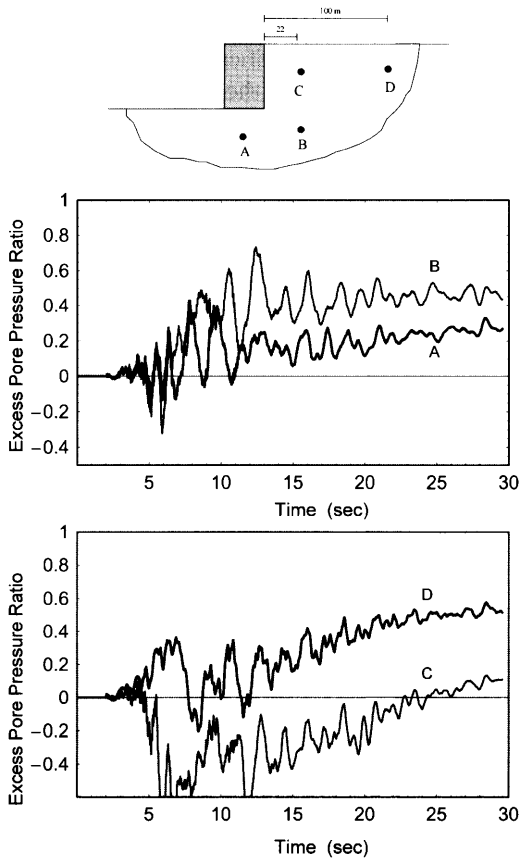

Fig. 13. Case 2: Densified soil of the backfill ($D_r = 75\%$) and the foundation ($D_r = 75\%$): Computed excess porewater pressure ratio $\Delta u/\sigma'_{0m}$ at points A, B, C, and D

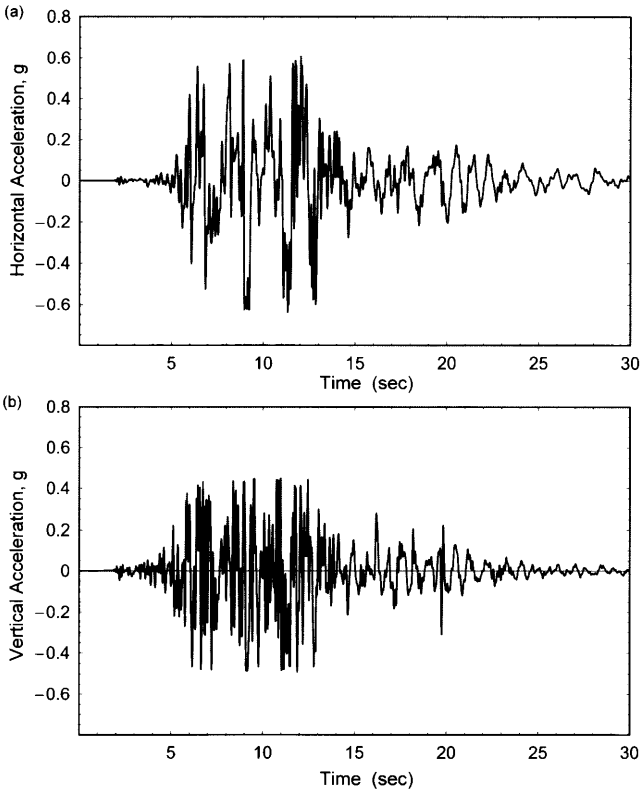

Fig. 14. Case 2: Densified soil of the backfill ($D_r = 75\%$) and the foundation ($D_r = 75\%$): Computed (a) horizontal and (b) vertical acceleration time histories at the upper seaside corner of the caisson (point E of Fig. 4(b))

behavior in Rokko and Port Islands. Specifically, it was indeed observed that: (a) no liquefaction occurred near the quay-wall which failed; (b) liquefaction occurred in the unimproved fill material at the free field; (c) all the walls moved and rotated outward (seaward); and (d) the soil surface in front of the toe of the wall heaved substantially (e.g., Towhata et al., 1996; Ishihara et al., 1996; Inagaki et al., 1996).

Moreover, the numerical values computed with the modified Pastor model in conjunction with the finite-difference (FD) algorithm are in general agreement with earlier results presented by Iai et al. (1998) based on a different constitutive model and a finite-element (FE) formulation. Note that the latter analysis used 20 sec of the earthquake in which the upper left corner of the wall moved 3.5 m seaward, whereas in the present analysis the movement at that same time is about 2.8 m. Pore pressure ratios in the free field, however, are about 0.90 and 0.80, respectively in *both* analyses. Finally, there is a difference between the two analyses in the response at point C which lies within the active wedge of the two walls: our analysis shows that negative pore water pressures develop at that point, between 5 and 10 seconds, apparently the result of horizontal extension.

Case Study 2

In this case both the foundation and backfill soil are assumed to consist of dense sand, having the same constant relative density of $D_r = 75\%$. Figure 11(a) plots the deformed shape and the horizontal displacement contours of the quay-wall and Fig. 12 plots the horizontal and vertical displacement time histories at point E (Fig. 4(b)). Notice that the soil improvement leads to a reduction of the maximum horizontal displacement to 2.1 m, from the 3.95 m of Case 1. The settlement at point E is reduced from 1.3 m to 0.5 m. The settlement behind

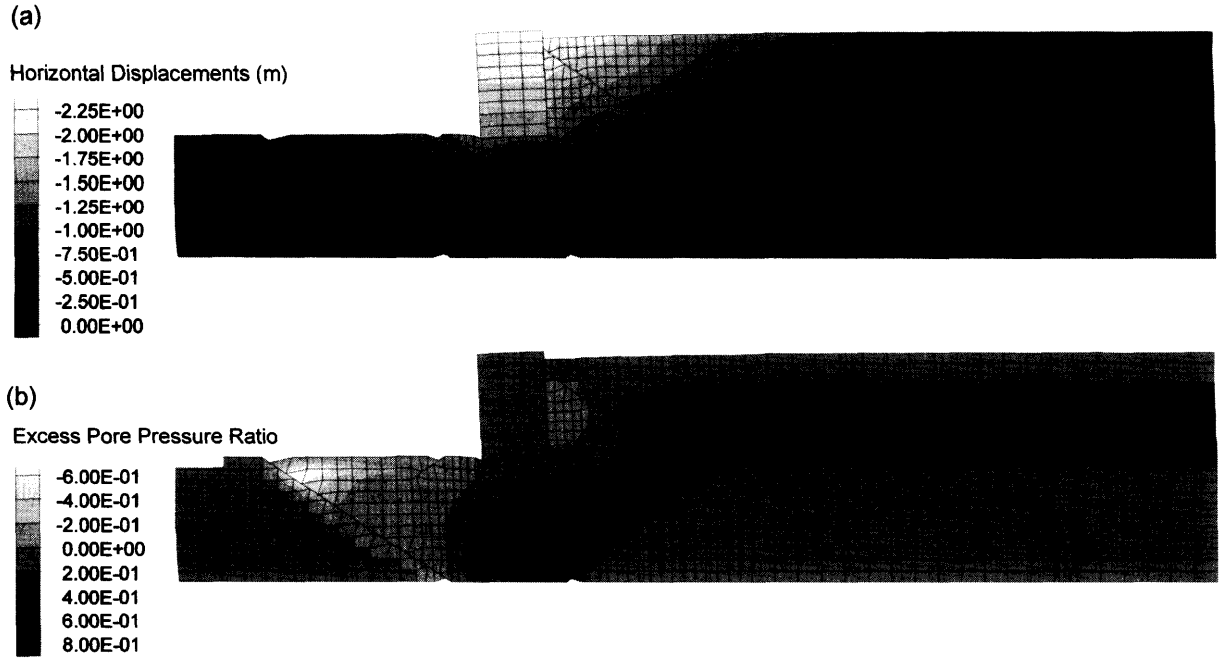

Fig. 15. Case 3: Densified foundation soil (only): (a) Deformed geometry and contours of horizontal displacements of the quay wall at the end of shaking ($t = 30$ sec) and (b) Contours of excess porewater pressure ratio for the foundation and backfill zones at the end of shaking ($t = 30$ sec)

the wall is 0.9 m.

Figure 11(b) plots contours of the excess porewater pressure ratio $\Delta u/\sigma'_{0m}$, whereas the time histories at points A, B, C, and D are plotted in Fig. 13. Evidently, the dense soil suffers smaller positive excess porewater pressures and (in absolute terms) larger negative excess porewater pressures. The excess porewater pressure ratio in the free field is increasing with time, but at a slower rate compared to values in Case 1, leading to an accumulation of 0.50 at the end of the earthquake. The ratios at A and B are nearly 0.30 and 0.40, respectively. Point C, located 22 m from the wall back, experiences negative pressures of up to ≈ 24 sec, and only in the last 6 sec does it reach positive values.

Of great significance is the observation that there is still a significant horizontal displacement of the quay-wall despite the fact that both foundation and backfill consist of improved soil. This is due to the substantially higher accelerations that can be transmitted through the soil and thereby develop on the wall in this case, and the inadequacy of the wall design to sustain such a strong ground shaking without significant rotation due to large outward overturning moments. Figure 14 plots the horizontal and vertical acceleration time histories at point E, with peaks of about 0.62 g and 0.50 g, respectively. Without paying too much attention to the isolated high-frequency spikes in the time histories of Figs. 14 and 9 (which are perhaps a somewhat spurious outcome of numerical integration), it is clear that the accelerations of the wall are about 1.40 times higher in this case of fully improved soil (Fig. 14) than in the case of the original soil (Fig. 9).

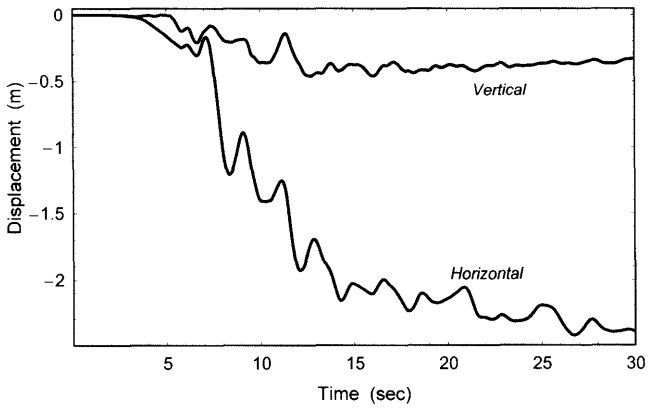

Fig. 16. Case 3: Densified foundation soil (only): Computed horizontal and vertical displacement time histories for the upper seaside corner of the caisson

Case Study 3

In Case 3 the equivalent relative density in the improved foundation soil is taken equal to $D_r = 75\%$, while in the backfill soil is $D_r = 35\%$. Note that in the quay-wall sections PC-14 and PC-15 in Port Island, the foundation soil had been improved using the sand compaction pile method, whereas the backfill soil consisted of loose saturated sand. As material properties and geometry of these sections may be approximated by those in Case 3, the computed response may be compared to the observed response at sections PC-14 and PC-15. Figure 15(a) plots the deformed shape and the horizontal displacement contours of the quay-wall. Figure 16 plots the horizontal and vertical displacement time histories at point E. The improved foundation soil results into a reduction of the

maximum horizontal displacement to 2.4 m and of the settlement to 0.5 m, compared to those in Case 1. However, the settlement in Case 3 is similar to that in Case 2, as both cases correspond to similar conditions in the foundation soil. The results are in agreement with the horizontal displacements of 2.5 m and vertical displacements of 0.3 m observed at the quay-wall sections PC-14 and -15 of Port Island (Iai et al., 1998). Figure 15(b) plots the contours of the excess porewater pressure ratio $\Delta u/\sigma'_{0m}$, and Fig. 17 plots the time histories of points A, B, C, and D. Note that the pore pressure response in the free field is, naturally, comparable to that in Case 1. The excess porewater pressure ratio at the shallow left part of the foundation soil, located between section aa and the alluvial clay zone 5 (*see* Fig. 4(b)), shows a more dilative response compared to the results from Case 2, due to the higher level of shearing induced by the backfill soil and the caisson wall.

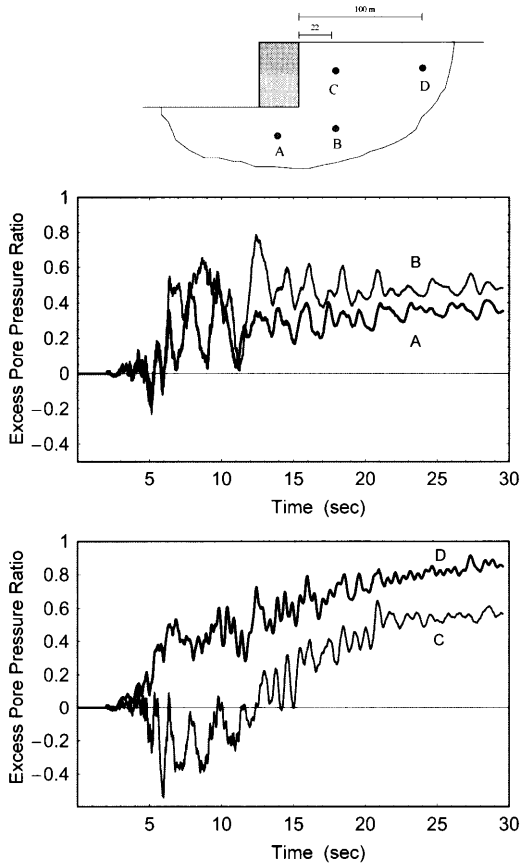

Fig. 17. Case 3: Densified foundation soil (only): Computed excess porewater pressure ratio $\Delta u/\sigma'_{0m}$ at points A, B, C and D

Case Study 4

This last case corresponds to a quay-wall, in which the foundation has a relative density of $D_r = 35\%$, whereas the backfill soil has been improved to a relative density

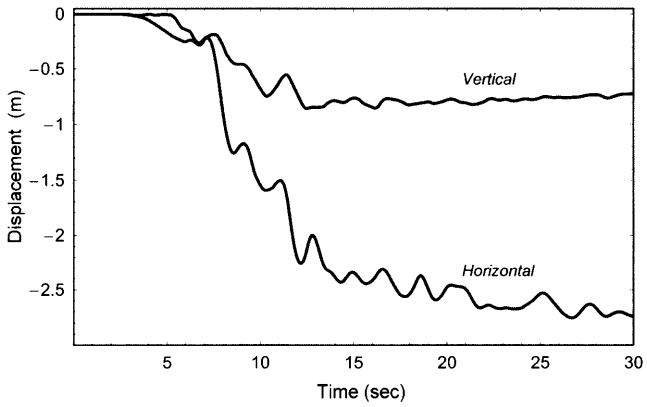

Fig. 19. Case 4: Densified backfill soil (only): Computed horizontal and vertical displacement time histories at the upper seaside corner of the wall

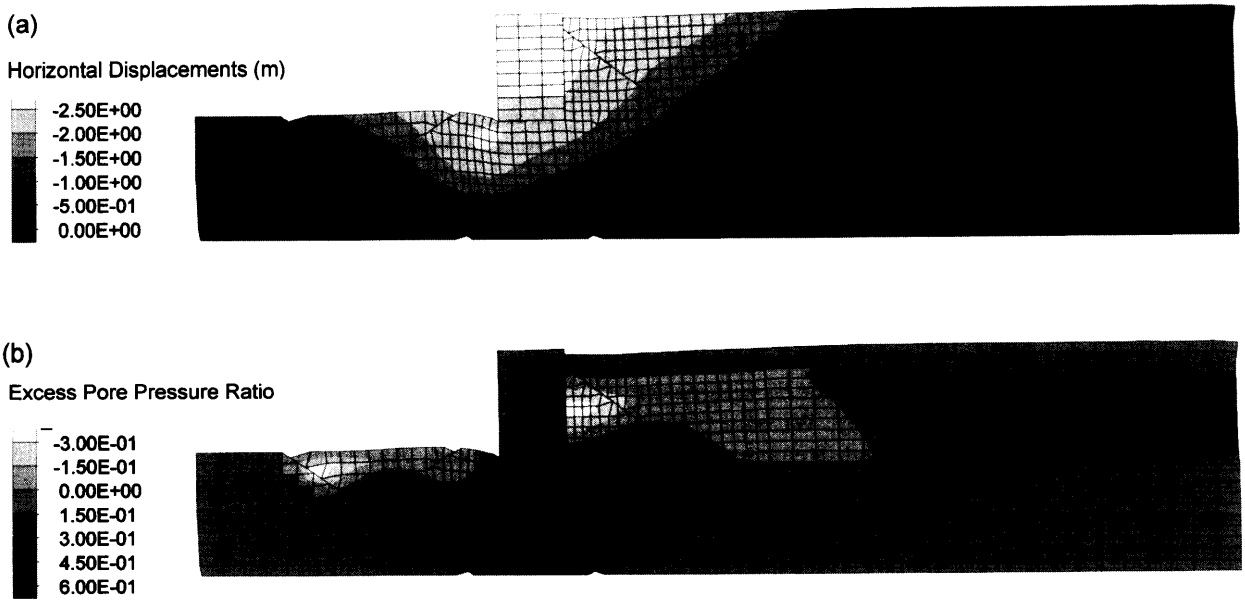

Fig. 18. Case 4: Densified backfill soil (only): (a) Deformed geometry and contours of horizontal displacements of the quay-wall at the end of shaking ($t = 30$ sec) and (b) Contours of excess porewater pressure ratio for the foundation and backfill zones at the end of shaking ($t = 30$ sec)

Table 3. Summary of computed wall displacement and rotation

Case	Relative density		Wall displacement (m)		Wall rotation (degrees)
	Foundation	Backfill	Horizontal	Vertical	
1	35%	35%	3.95	1.3	1.8°
2	75%	75%	2.1	0.5	1.5°
3	75%	35%	2.4	0.5	1.6°
4	35%	75%	2.7	0.9	0.6°

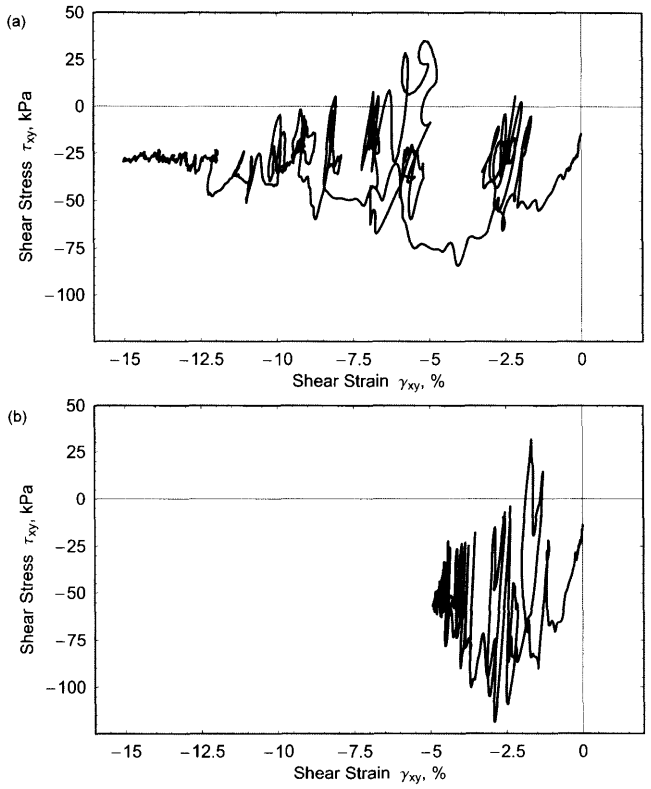

Fig. 20. Shear stress versus shear strain relationship at point F for (a) Case 1 and (b) Case 2

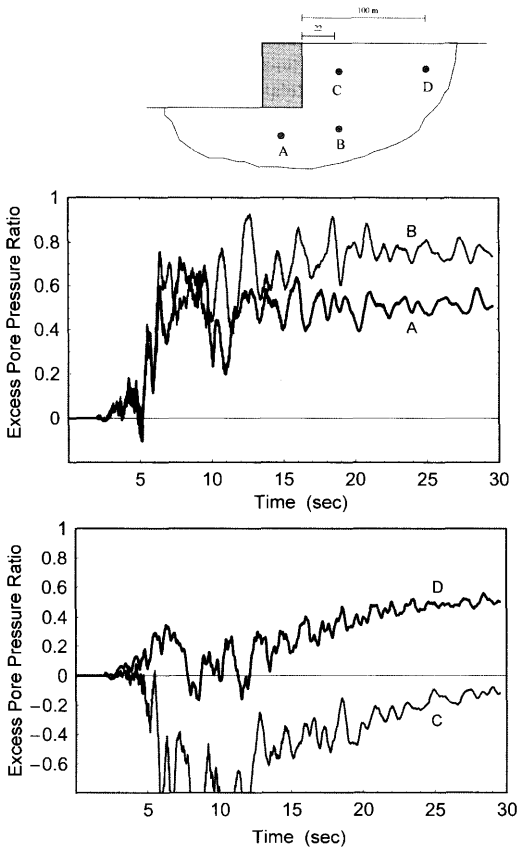

Fig. 21. Case 4: Densified backfill soil (only): Computed excess porewater pressure ratio $\Delta u/\sigma'_{0m}$ at points A, B, C and D

$D_r = 75\%$. Figure 18(a) plots the horizontal displacement contours of the quay-wall and Fig. 19 plots the horizontal and vertical displacement time histories at point E. The residual horizontal displacement at point E is 2.8 m and the settlement 0.9 m, whereas the settlement behind the wall is 1.4 m. Comparison of the results from Cases 1 and 4 shows similar significant shearing of the foundation soil and rubble due to reduction of the bearing capacity during shaking. By contrast, in Cases 2 and 3, the improved foundation soil deforms to a much lesser degree. This may be seen for example, in Fig. 20, which plots the shear stress τ_{xy} versus the shear strain γ_{xy} relationship at point F in the foundation soil beneath the caisson (*see* also Fig. 4(b)). The results demonstrate the effects of soil improvement in reducing the shear strain γ_{xy} in the foundation soil from about 15% in the loose soil of Case 1 to about 5% in the improved soil of Case 2. In addition, significantly higher shear stresses τ_{xy} are computed in the improved foundation soil due to the higher level of ground motion that is transmitted to the caisson wall, compared to the one transmitted in the case of loose foundation soil.

Moreover, in comparison with the results from Case 3, it suggests that improvement of the foundation soil is more effective in reducing permanent deformations than improvement of the backfill soil. The distribution of $\Delta u/\sigma'_{0m}$ in Fig. 18(b) shows high pore pressures at the more contractive, right part of the foundation soil, and negative values at the dilative left part, due to low confining stress and significant shearing. A summary of the computed response values is given in Table 3.

Comparison of wall rotations between Case 2 and Case 4 appears to suggest that Case 4 is more effective in reducing rotation. In reality, the rotation of the caisson

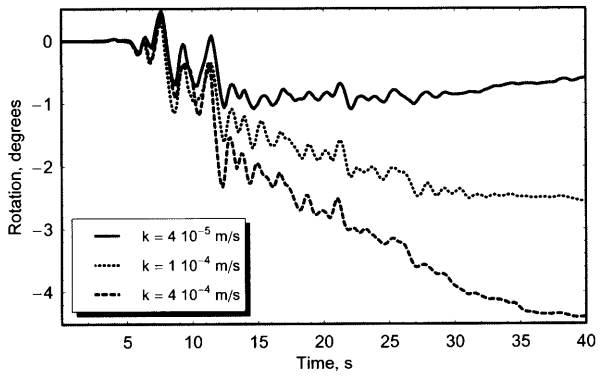

Fig. 22. Effect of the permeability of the foundation and backfill rubble on the caisson rotation (Relative density of foundation and backfill soils $D_r = 35\%$, Relative density of rubble material $D_r = 60\%$)

wall is controlled by many factors, including the combined action of the dilative behavior and the permeability of the backfill and foundation rubble material. As a demonstrative example, Fig. 22 plots the evolution of rotation for three walls, all having soil with relative density $D_r = 35\%$ in both the foundation and backfill soils and $D_r = 60\%$ in the foundation and backfill rubble. The walls differ only in the permeability of the foundation and backfill rubble material, which are taken alternately equal to $k = 4 \times 10^{-5}$, 10^{-4} and 4×10^{-4}. The results show that, in this case, higher permeability allows larger wall rotations, which for $k = 4 \times 10^{-4}$ reach values of about 4 degrees at the end of shaking. However, the rotation of the wall is also significantly dependent on the relative density and the associated dilative or contractive behavior of the foundation and rubble material. The results of an in-depth investigation on the rotation of caisson walls are beyond the scope of this paper.

CONCLUSIONS

An effective-stress method of analysis based on an extended version of the elasto-plastic constitutive model of Pastor (1990), is adapted into a finite-difference algorithm. The method is applied to re-analyze a typical Rokko Island quay-wall that experienced very large displacements during the 1995 Kobe earthquake (Case 1), and three idealized case studies (Cases 2, 3, and 4) of quay-walls, supporting and/or founded on improved ground.

For the Rokko Island quay-wall the computed permanent horizontal displacements (3.95 m) and settlements (2.1 m) of the wall and backfill soil are in accord with field observations. Similarly, the results of Case 3 approximate reasonably well the performance of sections PC-14 and -15 at Port Island which had improved foundation soil. The results show clearly that the model can capture the stress-change and density dependent *contractive* or *dilative* behavior of the foundation and backfill soils.

For Cases 1 and 4, in which the foundation is liquefiable, the analyses showed significant shearing of the foundation soils, accompanied by development of high pore water pressures, and reduction in bearing capacity. In Cases 2 and 3 the improved foundation soil is sheared to a much lesser degree.

The excess pore pressure away from the wall attains the expected free-field values, leading either to liquefaction, in case of loose sand backfill, or to cyclic mobility in case of dense sand backfill. In agreement with field observations, no liquefaction occurs within a zone about 30 m from the back of the wall, due to the predominant reduction in lateral stresses and the ensuing negative porewater pressures as the wall moved seaward.

A perhaps surprising result is that even for Case 2, in which both the foundation and backfill soil have been substantially improved to $D_r \approx 75\%$ and are thus nonliquefiable, lateral wall displacement and rotation attained the significant values of 2.1 m and 1.5°, respectively. The culprit is the higher acceleration that could be transmitted through the stiffer soil, thereby producing larger inertial forces and overturning moments at the caisson base; this compensated for the larger porewater pressures of Case 1.

The results for all four cases are in accord with the results of earlier similar analyses using a different constitutive model and the FE formulation presented by Iai et al. (1998).

REFERENCES

1) Castro, G. (1969): Liquefaction of sands, *Ph.D. Thesis*, Harvard University, *Harvard Soil Mechanics Series*, No. 81.
2) Cubrinovski, M. and Ishihara, K. (1999): Empirical correlation between SPT *N*-value and relative density for sandy soils, *Soils and Foundations*, **39**(5), 61-71.
3) Cubrinovski, M. and Ishihara, K. (2000): Flow potential of sandy soils with different grain compositions, *Soils and Foundations*, **40**(4), 103-119.
4) Cubrinovski, M. and Ishihara, K. (2001): Correlation between penetration resistance and relative density of sandy soils, *Proc. 15th ICSMGE*, Istanbul, Turkey, 393-396.
5) Dakoulas, P. (2003a): Seismic analysis of gravity quay walls, *Proc. Int. Workshop IWS-Athens "Prediction and Simulation in Geomechanics"*, 14-15 October 2003, Athens, Greece.
6) Dakoulas, P. (2003b): Verification of a constitutive model for non-cohesive soils, *Research Report*, University of Thessaly, Volos, Greece (in Greek).
7) DeAlba, P., Seed, H. B. and Chan, C. K. (1976): Sand liquefaction in large scale simple shear tests, *J. Geotech. Engrg. Div.*, ASCE, **102**(9), 909-927.
8) Dickenson, S. and Yang, D. S. (1998): Seismically-induced deformations of caisson retaining walls in improved soils, *Geotechnical Earthquake Engineering and Soil Dynamics III* (eds. by Dakoulas, P., Yegian, M. K. and Holtz, R. D.), Geotechnical Special Publication, No. 75, ASCE, **2**, 1071-1082.
9) Fujiwara, T., Horikoshi, K. and Sueoka, T. (1999): Centrifuge modeling of dynamic earth pressure acting on gravity type wall during large earthquake, *Proc. 2nd Int. Conf. Earthquake Geotech. Engrg.* (ed. by Pedro Seco e Pinto), Lisbon, **1**, 401-406.
10) Gazetas, G., Dakoulas, P. and Dennehy, K. (1990): Empirical seismic design method for waterfront anchored sheetpile walls, *Design and Performance of Earth Retaining Structures*, ASCE, 232-250.
11) Ghalandarzadeh, A., Orita, T., Towhata, I. and Yun, F. (1998): Shaking table tests on seismic deformation of gravity quay-walls,

Soils and Foundations, Special Issue on Geotechnical Aspects of the January 17, 1995 Hyogoken-Nambu Earthquake, (2), 115–132.
12) Iai, S. (1998): Seismic analysis and performance of retaining structures, *Geotechnical Earthquake Engineering and Soil Dynamics III*, (eds. by Dakoulas, P., Yegian, M. K. and Holtz, R.), Geotechnical Special Publication, No. 75, ASCE, Vol. II, 1020–1044.
13) Iai, S., Ichii, K., Liu, H. and Morita, T. (1998): Effective stress analysis of port structures, *Soils and Foundations, Special Issue on Geotechnical Aspects of the January 17, 1995 Hyogoken-Nambu Earthquake*, (2), 97–114.
14) Inagaki, H., Iai, S., Sugano, T., Yamazaki, H. and Inatomi, T. (1996): Performance of caisson type quay walls at Kobe port, *Soils and Foundations, Special Issue of Geotechnical Aspects of the January 17, 1995 Hyogoken-Nambu Earthquake*, (1), 119–136.
15) Ishihara, K. (1997): Terzaghi oration: Geotechnical aspects of the 1995 Kobe earthquake, *Proc. 14th ICSMFE, Hamburg,* **4**, 2047–2073.
16) Ishihara, K., Yasuda, S. and Nagase, H. (1996): Soil characteristics and ground damage, *Soils and Foundations, Special Issue of Geotechnical Aspects of the January 17, 1995 Hyogoken-Nambu Earthquake*, (1), 109–118.
17) Ishihara, K., Yoshida, K. and Kato, M. (1997): Characteristics of lateral spreading in liquefied deposits during the 1995 Hanshin-Awaji earthquake, *J. Earthquake Engineering*, **1**, 23–55.
18) Itasca Consulting Group (2000): *Fast Lagrangian Analysis of Continual*, User's Manuals, Minneapolis, MN, USA.
19) Iwasaki, Y. and Tai, M. (1996): Strong motion records at Kobe Port Island, *Soils and Foundations, Special Issue of Geotechnical Aspects of the January 17, 1995 Hyogoken-Nambu Earthquake*, (1), 29–40.
20) Kamon, M., Wako, T., Isemura, K., Sawa, K. Mimura, M., Tateyama, K. and Kobayashi, S. (1996): Geotechnical disasters on the waterfront, *Soils and Foundations, Special Issue of Geotechnical Aspects of the January 17, 1995 Hyogoken-Nambu Earthquake*, (1), 137–147.
21) Kitajima, S. and Uwabe, T. (1978): Analysis on seismic damage in anchored sheet-piling bulkheads, *Report of the Port and Harbor Research Institute*, **18**(1), 67–130 (in Japanese).
22) Kuwano, J., Takahashi, A., Hiro-oka, A. and Yamauchi, K. (1999): Shaking table tests on caisson type quay wall in centrifuge, *Proc. 2nd Int. Conf. Earthquake Geotech. Engrg.* (ed. by Pedro Seco e Pinto), Lisbon, **1**, 365–370.
23) Ling, H. and Liu, H. (2003): Pressure-level dependency and densification behavior of sand through generalized plasticity model, *J. Engrg. Mech.*, ASCE, **129**(8), 851–860.
24) Pastor, M. and Zienkiewicz, O. (1986): A generalized plasticity hierarchial model for sand under monotonic and cyclic loading, *Numerical Methods in Geomechanics* (eds. by Pande, G. N. and Impe, W. F.), Jacjson, London, 131–150.
25) Pastor, M., Zienkiewicz, O. and Leung, K. H. (1985): Simple model for transient soil loading in earthquake analysis II: Non-associative models for sands, *Int. J. Numerical and Analytical Methods in Geomechanics*, **9**(5), 477–498.
26) Pastor, M. O., Zienkiewicz, O. and Chan, C. H. (1990): Generalized plasticity and the modeling of soil behavior, *Int. J. Numerical and Analytical Methods in Geomechanics*, **14**, 151–190.
27) PIANC (2001): *Seismic Design Guidelines for Port Structures*, International Navigation Association, A. A. Balkema Publishers, 474.
28) Sawada, S. and Kondoh, M. (1999): Seismic retrofit design using steel sheet pile with wedge shape head, *Proc. 2nd Int. Conf. Earthquake Geotech. Engrg.*, (ed. by Pedro Seco e Pinto), Lisbon, **1** 353–358.
29) Sekiguchi, H., Koyama, M., Takebe, A., Yamada, H. and Miyamoto, J. (1999): A seismic reinforcement of gravity-type quaywalls, *Proc. 2nd Int. Conf. Earthquake Geotech. Engrg.*, (ed. by Pedro Seco e Pinto), Lisbon, **1** 389–394.
30) Seed, R. B. and Harder, L. F. (1990): SPT-based analysis of cyclic pore pressure generation and undrained residual strength, *Proc. H. B. Seed Memorial Symp.*, **2**, 351–376.
31) Tazoh, T. and Gazetas, G. (1996): Pile foundations subjected to large ground deformations: lessons from Kobe and research needs, *Proc. 11th World Conf. on Earthquake Engrg.*, Acapulco, Mexico, paper No. 2081.
32) Torii, T. and Tatsuoka, F. (1982): A study of triaxial liquefaction strength of gravelly soil, *Proc. Annu. Meet.*, JSSMFE, 1669–1672.
33) Towhata, I., Ghalandarzadeh, A., Sundarraj, K. and Vargas-Monge, W. (1996): Dynamic failures of subsoils observed in waterfront areas, *Soils and Foundations, Special Issue of Geotechnical Aspects of the January 17, 1995 Hyogoken-Nambu Earthquake*, (1), 149–160.
34) Zienkiewicz, O. C., Leung, K. H. and Pastor, M. (1985): Simple model for transient soil loading in earthquake analysis I: Basic model and its application, *Int. J. Numerical and Analytical Methods in Geomechanics*, **9**(5), 453–476.
35) Zienkiewicz, O. C., Pastor, M., Chan, C. and Xie, Y. (1991): Computational approaches to the dynamics and statics of saturated and unsaturated soils, *Adv. Geot. Anal., Devel. in SMFE 4*, (eds. by Banerjee, P. and Butterfield, R.), Elsevier, 151–190.
36) Zienkiewicz, O. C., Chan, C., Pastor, M., Schrefler, B. A. and Shiomi, T. (1999): *Computational Geomechanics with Special Reference to Earthquake Engineering*, J. Wiley, NY, 383.